ISSN: 2688-8645

Optimization Design of Sand Washer Based on CFD-DEM Coupling

Yi Zhang, Zhen Wang, Daqin Zhang, Bangyao Tang

School of Mechanical and Electrical Engineering, Southwest Petroleum University, Chengdu Sichuan, 610500, China

Abstract

Sand washers play a crucial role in the oil drilling field. To improve the drilling cuttings screening efficiency of sand washers, it is necessary to optimize the structure of the sand washer's vibrating screen. This paper takes the vibrating screen of the sand washer as the research object and investigates how its screening performance is affected by multiple factors such as amplitude, frequency, vibration mode, and screen mesh. Firstly, the CFD-DEM method is adopted for numerical simulation to study the influence of the vibration parameters of the sand washer's vibrating screen on the screening efficiency. Secondly, in order to achieve the optimal drilling cuttings screening efficiency, a response surface optimization analysis with the maximum screening efficiency as the optimization objective is established using the simulation results under different parameters, and the optimal combination of various parameter values is determined. Finally, the reliability of the numerical simulation is verified by comparing the results of the sand washer experiment with the numerical simulation results.

Keywords

CFD-DEM; Vibrating Screen; Response Surface Optimization; Sand Washer; Numerical Simulation.

1. Introduction

During the drilling process, drilling fluid carries the rock fragments crushed by the drill bit from underground to the surface. These rock fragments mixed in the drilling fluid are called drilling cuttings. Continuously obtained drilling cuttings can directly describe the formation geological section, reflect the downhole formation conditions and rock properties, and provide an initial understanding of the oil and gas-bearing status of the formation. With the advantages of low cost, simple operation, timely reflection of downhole conditions, and systematic data, it serves as an effective cognitive tool for geological logging [1]. The sand washer is a key logging equipment in the drilling process, whose function is to effectively screen out cuttings particles from drilling fluid to ensure the smooth progress of subsequent logging operations. To investigate the factors influencing the screening efficiency of the sand washer, it is necessary to modify the structural parameters of the vibrating screen, thereby improving the drilling cuttings screening efficiency of the sand washer. However, the vibrating screening effect of the sand washer is closely related to the structural parameters of the equipment; therefore, the reasonable optimization of vibration parameters is crucial for enhancing the screening efficiency.[2]. Due to the presence of drilling cuttings with varying particle sizes in the drilling fluid, the vibrating screen mesh of the sand washer has been specially designed. The vibrating screen mesh of the sand washer is divided into three layers, which sequentially screen large, medium, and small-sized cuttings particles from top to bottom, while the drilling fluid flows out through the bottom outlet. The designed multi-layer vibration model of the sand washer is illustrated in Fig. 1. [3].

ISSN: 2688-8645

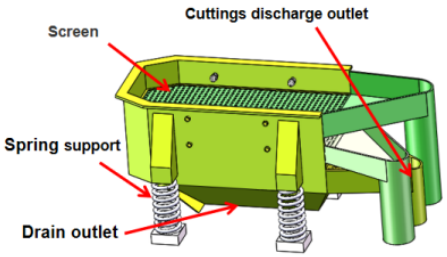

Fig 1. Simple multi-layer vibration model.

Vibrating screens are one of the key equipment for particle separation. They utilize the particle size difference among particles to perform screening and obtain the target particles we need, and the vibration parameters and working modes of vibrating screens have a significant impact on the screening effect. Liu et al. used the discrete element software EDEM to simulate the motion behavior of mixed particles on a double-layer linear vibrating screen and discussed the influence laws of different factors on the screening effect of the vibrating screen. Zhipeng Lyu et al. proposed a new type of vibration trajectory, the spatial Lissajous trajectory, and established a corresponding vibrating screen model. In the experiment, EDEM software was adopted to simulate the motion behavior of binary mixed particles on the spatial Lissajous vibrating screen, and two sets of comparative experiments with different vibration trajectories were set up: linear trajectory and elliptical trajectory. [4-6]The results showed that when the vibration trajectory is elliptical, the particle motion velocity is the smallest; when the vibration trajectories are spatial Lissajous and linear, the particle motion velocities are almost the same, but the spatial Lissajous vibrating screen has relatively better screening efficiency and is less prone to screen hole clogging. This advantage is particularly prominent when screening water-containing particles.[7].

Not only do particle density and particle size affect the separation effect of mixed particles, but particle shape is also crucial for the particle separation effect. Wang et al. [8] adopted the multi-sphere packing method to establish 11 types of non-spherical particles in EDEM software, with the particle shapes showing a continuous gradient law. By changing parameters such as the vibration frequency, amplitude, and vibration direction angle of the vibrating screen, and taking separation efficiency as the evaluation criterion, they quantitatively analyzed the influence of particle shape on the particle separation effect. The results showed that within a fixed time, as the particle shape gradually changes from cubic to flaky and then from flaky to cylindrical, the particle screening efficiency varies from 15% to 25%, and the screening efficiency of non-spherical particles is relatively low. Moreover, the result analysis indicated that the variation trend of screening efficiency of particles with different shapes under different process parameters is consistent.[9].

M.R. Fatahi et al. used Fluent software to simulate the liquid-solid two-phase flow in the separator and obtained the influence law of water flow velocity and pressure distribution in the separation chamber on the separation effect of mixed particles. Zhang et al. conducted simulation research on the separation behavior of multi-component mixed particles in a pulsed fluidized bed based on ANSYS-FLUENT software using the two-fluid model. The results showed that pulsed flow excitation is beneficial to improving the separation efficiency of mixed particles, but when the pulsed frequency exceeds a certain critical value, the particle separation effect will weaken, and the separation efficiency will gradually decrease with the increase of particle size. The combination of Computational Fluid Dynamics (CFD) and Discrete Element Method (DEM) has been widely used in numerical simulation of two-phase flow. To simulate the influence of particle flow characteristics in drilling fluid, the CFD-DEM method can be adopted to predict the interaction characteristics between fluid and particles in two-phase flow. Liang [12] et al. studied the influence of operating parameters on the spin and heat transfer of

ISSN: 2688-8645

sludge particles in a cyclonic self-rotating drying device, and the results indicated that the particle spin velocity and rotational speed decrease with the increase of particle size and feed rate; Shan [13] investigated the motion trajectory and erosion ratio law of particles in T-shaped pipelines during heavy oil migration; Mazen [14] studied the influence of the distance between two strings of elbows on the erosion of solid particles on the elbows through numerical simulation and experiments. In addition, in practical applications, particle materials are usually non-spherical [15]. Li [16] et al. analyzed the influence of particle sphericity on the flow and erosion of hydraulically transported pipelines. Meng [17] summarized the factors affecting the pipe wall erosion rate, including the velocity of particles entering the pipeline, particle size, and pipeline material properties. Pavel [18] et al. studied the influence of solid concentration and mixture velocity on the pressure drop and concentration distribution of particle-water mixtures.

Based on the above analysis, this paper will consider the influence of drilling fluid on drilling cuttings during the vibrating screening process of the sand washer. Using the CFD-DEM coupling analysis method, a prediction model for the performance parameters of the sand washer will be established based on the simulation data through response surface optimization, aiming to maximize the screening efficiency while ensuring the sand washer normally screens drilling cuttings from the drilling fluid[19-23].

2. Model Description

2.1. Physical Model

To facilitate the simulation analysis of the screening process of the sand washer's vibrating screen, its model structure is simplified and scaled down proportionally, as shown in Fig. 2. The sand washer model has a height (h) of 100 mm, a length (a) of 150 mm, an inlet diameter (d) of 4 mm, and a width (b) of 90 mm. The distance between each two layers of the vibrating screen (h1) is 12 mm, and the angle between the screen mesh and the horizontal direction (α) is 5°. These settings are intended to facilitate the simulation analysis of the vibrating screening performance of the sand washer[24].

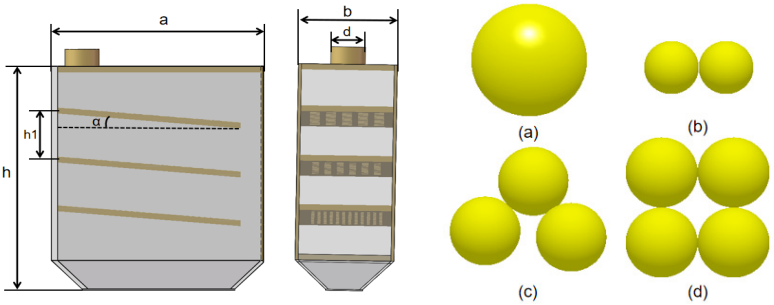

Fig 2. multi-layer vibration model and particle simulation model.

Table 1. Material properties.

Classification	Physical Parameter	Unit	Value
drilling fluid	density	g/cm³	1.5
	dynamic viscosity	mPa·s	25
Particle	diameter	mm	4/2.4/1.2/0.7
	density	Kg/m³	2650
	Poisson's ratio		0.3
exposure parameter	Sliding friction coefficient between particle and wall	mm	0.3
	particle-particle rolling friction coefficient	mm	0.3
	coefficient of restitution		0.9

ISSN: 2688-8645

The particle size of drilling cuttings in the drilling fluid mainly ranges from 0.4 mm to 4 mm. In this paper, particles with diameters of 0.7 mm, 1.2 mm, 2.4 mm, and 4 mm (in ascending order) are selected for simulation. A coupling interface program will be developed to achieve the coupling between Fluent and EDEM software. Combined with the performance parameters of the drilling fluid, the influence of the structural parameters of the sand washer's vibrating screen and the inlet flow velocity of the drilling fluid on the drilling cuttings screening efficiency of the vibrating screen is simulated and analyzed. The parameters of the drilling fluid and particles are listed in Table 1.

2.2. Fundamental Formulae

The drilling fluid exhibits a certain viscosity during its flow in the sand washer[25]. Therefore, this paper adopts the standard k-epsilon model established by Launder and Spalding for numerical simulation and analysis. This model features stable performance and high calculation accuracy, and the influence of particles on turbulence is not considered in the simulation process [26]. The turbulent kinetic energy and turbulent kinetic energy dissipation rate can be expressed as:

$$\frac{\partial(\rho_w k)}{\partial t}+\frac{\partial(\rho_w k u_i)}{\partial x_j}=\frac{\partial}{\partial x_j}[(\mu_1+\frac{\mu_t}{\sigma_k})\frac{\partial k}{\partial x_j}]+G_k+G_b-\rho_w e-Y_m+S_k \tag{1}$$

$$\frac{\partial(\rho_w e)}{\partial t}+\frac{\partial(\rho_w e u_i)}{\partial x_j}=\frac{\partial}{\partial x_j}[(\mu_1+\frac{\mu_t}{\sigma_e})\frac{\partial \varepsilon}{\partial x_j}]+C_{1e}\frac{e}{k}G_k+C_{2e}\rho_w\frac{e^2}{k}+S_e \tag{2}$$

Where k is the turbulent kinetic energy, e is the turbulent kinetic energy dissipation rate, u_i is the mean velocity, x_j is the spatial coordinate, μ_1 is the interlaminar flow viscosity coefficient, μ_t is the turbulence viscosity coefficient, G_k is the turbulent kinetic energy generated by velocity, G_b is the turbulence kinetic energy generated by the buoyancy force, Y_m denotes the contribution of the fluctuating expansion in the compressible turbulence to the total dissipation rate, C_{1e}, C_{2e}, σ_k and σ_e are empirical constants, S_k and S_e are source terms [27].

This paper ignores the bonding or rupture resulting from particle collisions in the discrete phase simulation and assumes no heat exchange occurs between the discrete phase of particles and the continuous phase of drilling fluid. The discrete phase in solid-liquid two-phase flow is characterized by DPM, which is computed through differential equations within the Lagrangian coordinate framework. The corresponding equation of motion is presented in Eqs. (3)-(4) [27-29]

$$m_p\frac{dv_p}{dt}=F_{p-f}+G_p+\sum F_{p-p} \tag{3}$$

$$I_p\frac{dw_p}{dt}=\sum T_{p=p} \tag{4}$$

Where m_p is the particle mass, kg; v_p is the particle velocity, m/s; I_p is the rotational inertia, kg·m^2; w_p is the particle angular velocity, rad/s; G_p is the particle gravitational force, N; F_{p-p} and F_{p-f} are the forces of particles by other particles and fluid, N; T_{p-p} is the torque of other particles on particles, N/m.

The particle contact model is a mathematical model with physical properties applied to collisions between particles. When a group of particles is subjected to external excitation, complex motion behaviors occur. During the movement, contacts and collisions take place between particles as well as between particles and the inner wall of the container. When two objects come into contact, contact forces are inevitably generated. However, in actual production, the contact conditions of particles vary under different production scenarios, so

ISSN: 2688-8645

different particle contact models need to be set according to practical situations, as shown in Table 2. The Hertz no-slip model in Table 2 is one of the most commonly used contact models in EDEM software[30]. It is widely applicable in most production practices, and the results calculated using this model are not only accurate but also the entire computation process is very efficient.

Table 2. Commonly used contact model

Contact model	Field of application
Hertz slipless model	Model of rigid body nonlinear contact force
Hertz-Mindlin model	Model of bonded particles to a certain extent
Linear spring model	Rigid body linear model
Rolling damping model	Model of resistance to rolling
Walton Braun model	A Linear Model of Deformable Particles

2.3. CFD Physical Field Model

A one-way coupling strategy is adopted for the fluid-particle coupling simulation in this study, meaning that the fluid affects particle motion while the feedback effect of particles on the fluid field is negligible. Therefore, the stable pure fluid physical field is first calculated and exported in Fluent, serving as the driving environment for particle motion in EDEM. On the premise of ensuring accuracy, this method can significantly reduce computational complexity and resource consumption, and is particularly suitable for the migration and separation behavior of particles in a given flow field, which is the focus of this study[31-33].

The flow of drilling fluid inside the sand washer follows the laws of mass conservation and momentum conservation, and its governing equations are as follows:

$$\frac{\partial \rho}{\partial t} + \nabla \cdot (\rho \vec{v}) = 0 \tag{5}$$

Given that drilling fluid can be regarded as an incompressible fluid with a constant densityρ, the governing equations are simplified as follows:

$$\nabla \cdot \vec{v} = 0 \tag{6}$$

where $\vec{v}$denotes the fluid velocity vector.

$$\frac{\partial(\rho\vec{v})}{\partial t} + \nabla \cdot \left(\rho\overrightarrow{\vec{v}\vec{v}}\right) = -\nabla p + \nabla \cdot \left(\mu_{eff}(\nabla\vec{v} + (\nabla\vec{v})^T)\right) + \rho\vec{g} + \overrightarrow{S_p} \tag{7}$$

Where ρ is the fluid pressure, $\vec{g}$ is the gravitational acceleration vector, and μ_{eff} is the effective viscosity. $\overrightarrow{S_p}$ is the momentum source term exerted by the particle phase on the fluid during subsequent coupling with DEM, and it constitutes the core of two - way coupling.

To simulate the resistance of the screen mesh to the fluid, the three - layer screen mesh region is defined as a porous medium. Its momentum source term $\overrightarrow{S_p}$ consists of a viscous loss term and an inertial loss term, expressed as follows:

$$\overrightarrow{S_i} = -\left(\frac{\mu}{\alpha}v_i + C_2\frac{1}{2}\rho|v|v_i\right) \tag{8}$$

where $\frac{1}{\alpha}$ is the viscous resistance coefficient and C_2 is the inertial resistance coefficient. Their values are estimated based on the Ergun equation, combined with the porosity and pore size of each screen layer, to accurately reflect the pressure drop caused by the screen mesh[34].

ISSN: 2688-8645

2.4. Boundary Conditions and Grid Independence Verification

CFD-DEM can simulate most fluid-particle systems. CFD first achieves convergence of calculations at a specific time step and transmits the flow field information to DEM through a coupling interface[35]. DEM then calculates the external forces acting on each particle and updates the particle motion states. Finally, the particle properties are fed back to CFD for calculation, and the next iteration is performed.

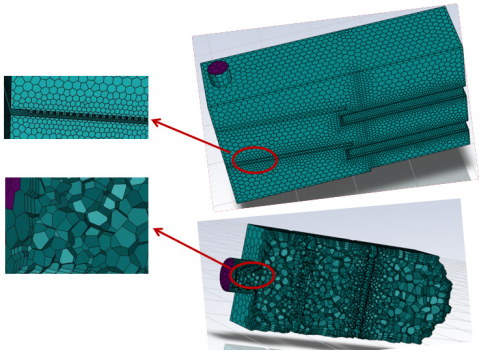

Fig 3. Grid Division Results

This study investigates the motion of drilling fluid in the sand washer, requiring grid division of the sand washer structure. For grid independence verification, the sand washer structure is divided into 5 grids with different quantities, as shown in Fig. 3, and the average velocity of screened particles is statistically analyzed. The simulation conditions are set as follows: viscosity of 25 mPa·s, density of 1.5 g/cm^3, inlet velocity of 1.5 m/s, particle diameter of 2 mm, and particle flow rate of 1000 n/s. To save computational resources, heat transfer is not considered. The time step in EDEM is set to 1.6×10^{-5} s, and the time step in CFD is set to 1.4×10^{-3} s. The calculation stops after 10 s, and the particle operating parameters and fluid parameters are kept consistent for each simulation.

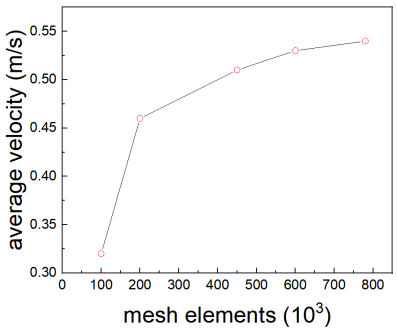

Fig 4. Grid Independence Verification

As can be seen from Fig. 4, changes in grid size significantly affect the accuracy of simulation calculations. The average particle velocity of coarse grids is obviously lower than that of fine grids. To ensure calculation accuracy and save computation time, the grid parameter with a grid number of 624,362 is selected as the computational grid for numerical simulation[36].

3. Results Analysis

3.1. Influence of Parameters on the Screening Efficiency and Performance of the Sand Washer

3.1.1. Influence of Vibrating Screen Frequency on Screening Efficiency

The vibration frequency of the screen mesh is one of the important parameters of the sorting device during operation, and it has a significant impact on the separation effect of mixed

ISSN: 2688-8645

particles. The motion state of particles on the screen mesh is closely related to the vibration frequency of the screen mesh: the higher the vibration frequency of the screen mesh, the more intense the particle motion on the screen surface, the number of contacts with the screen mesh will also increase, and their motion velocity will change accordingly[37]. Therefore, to study the influence of different vibration frequencies on the working process of the screen mesh, the frequency was taken as the test factor. Referring to the parameter settings in other relevant literature and actual working conditions, the initial parameter values were selected as follows: amplitude of 2 mm and screen surface inclination angle of 5°. A large number of preliminary experiments were conducted, with vibration frequencies set from low to high as 6 Hz, 8 Hz, 10 Hz, 12 Hz, and 15 Hz, respectively. The control variable method was adopted during the experiment to keep other parameters such as amplitude and vibration direction angle constant. The simulation process is shown in Fig. 5.

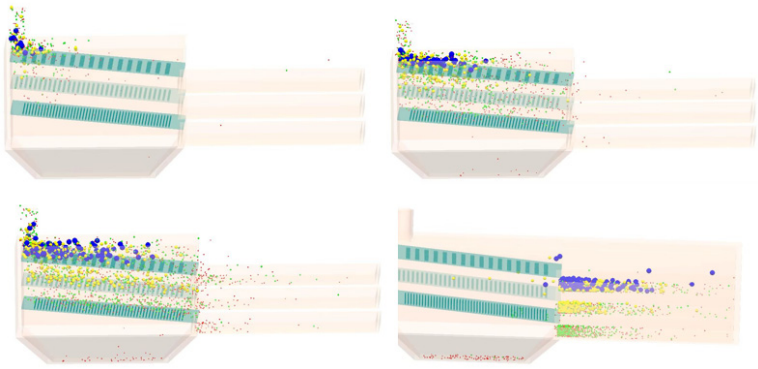

Fig 5. Simulation Process Diagram

After the simulation, the experimental data were processed and analyzed, and the particle motion velocity on the screen surface is shown in Fig. 6 below. Fig. 6 presents the average velocity distribution of particles at different frequencies. It can be clearly observed from the figure that there are significant differences in the average velocity distribution of particles under different frequencies. When the vibration frequency increases from 6 Hz to 15 Hz, the average motion velocity of particles on the screen surface increases from approximately 0.42 m/s to 0.61 m/s. Therefore, the average motion velocity of particles on the screen surface increases with the increase of the screen mesh vibration frequency.

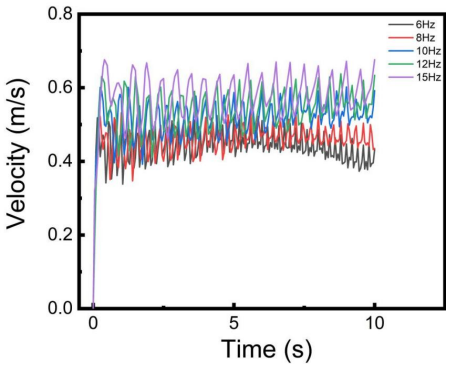

Fig 6. Average Particle Velocity at Different Frequencies

Fig. 7 is a bar chart of the recovery rate and impurity content of the sand washer at different vibration frequencies. As can be seen from the figure, the cuttings recovery rate first increases and then decreases with the increase of the screen mesh vibration frequency. When the vibration frequency is 8 Hz, the recovery rate reaches the maximum value of 92.8%. The cuttings impurity content first decreases and then slightly increases with the increase of the

ISSN: 2688-8645

screen mesh vibration frequency. When the vibration frequency is 8 Hz, the impurity content reaches the minimum value of 7.2%.

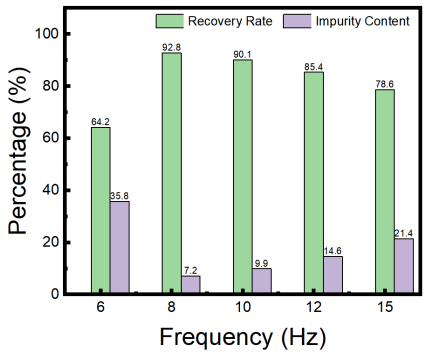

Fig 7. Particle Recovery Rate at Different Frequencies

Analysis: As shown in Fig. 7, the cuttings recovery rate increases significantly when the vibration frequency ranges from 6 Hz to 8 Hz, rising from 64.2% to 92.8%. This is because with the increase of the screen mesh vibration frequency, the motion of cuttings particles on the screen surface becomes more intense, and the contact between particles and the screen mesh becomes more frequent. Consequently, the number of small-sized particles passing through the screen holes gradually increases, leading to a higher collection volume of small-sized iron ore particles and a subsequent gradual rise in the cuttings recovery rate. When the vibration frequency further increases from 8 Hz to 15 Hz, the cuttings recovery rate shows a downward trend, decreasing from 92.8% to 78.6%. The reason is that although the number of contacts between particles and the screen mesh continues to increase with the rising vibration frequency, the motion velocity of particles on the screen surface also increases significantly. This causes more and more particles to be transported out of the screen mesh range without passing through the screen holes in time due to excessively high motion velocity, resulting in small-sized cuttings particles falling out from the upper layers of the screen.

3.1.2. Influence of Screen Mesh Amplitude on Screening Efficiency

The vibration amplitude of the sand washer's screen mesh is directly related to the energy acquired by cuttings particles on the screen surface. The smaller the vibration amplitude, the less energy the cuttings particles obtain. At this time, they are not easily lifted and remain on the screen surface, making it difficult for large, medium, and small-sized cuttings particles to stratify and pass through the screen. Therefore, the magnitude of the vibration amplitude affects the motion velocity of the cuttings particle group on the screen surface and the screening effect. To explore the influence of screen mesh vibration amplitude on the separation effect of mixed particles, the amplitude was taken as the test factor. Referring to the amplitude settings in other relevant literatures and actual working conditions, a large number of preliminary experiments were conducted, with five groups of tests designed. The amplitudes were set to 1 mm, 1.5 mm, 2 mm, 2.5 mm, and 3 mm respectively. Through the analysis of test data under different vibration frequencies, it was found that the optimal vibration frequency is 8 Hz. Thus, the vibration frequency was fixed at 8 Hz, and other parameters were kept constant.

The larger the vibration amplitude of the screen mesh, the more intense the motion state of particles on the screen surface, and the greater the particle motion velocity. As can be seen from Fig. 8, there are significant differences in the average motion velocity of particles under different amplitudes. With the increase of the screen mesh vibration amplitude, the average motion velocity of particles gradually increases. After the simulation, the test data were processed and analyzed, and the particle motion velocity on the screen surface is shown in Fig. 8 below. Fig. 8 presents the average velocity distribution of particles at different amplitudes. It can be clearly observed from the figure that there are obvious differences in the average

ISSN: 2688-8645

velocity distribution of particles under different amplitudes. When the vibration amplitude increases from 1 mm to 3 mm, the average motion velocity of particles on the screen surface increases from approximately 0.28 m/s to 0.57 m/s. Therefore, the average motion velocity of particles on the screen surface increases with the increase of the screen mesh vibration amplitude.

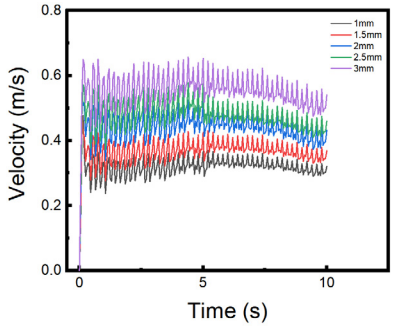

Fig 8. Average Particle Velocity at Different Amplitudes

As shown in Fig. 8, this is a curve chart of the average velocity of cuttings particles under different amplitudes. Compared with the velocity curve chart of cuttings particles at different vibration frequencies, the variation trend of the cuttings particle velocity curve is more discrete when the vibration amplitude changes. When the vibration amplitude is 1 mm, the average velocity range of cuttings particles is 0.25 m/s to 0.35 m/s. At this time, the displacement of the screen body is too small, and the reciprocating displacement of cuttings particles is also too small. They cannot obtain sufficient energy to maintain relative motion with the screen surface, leading to the easy accumulation of cuttings particles on the screen surface, which is not conducive to improving the screening efficiency. Excessively long residence time of cuttings particles on the screen surface will increase the mis-screening rate. When the vibration amplitude is 2 mm, the average velocity range of cuttings particles is 0.35 m/s to 0.49 m/s. With the increase of the screen body vibration amplitude, the acceleration time of cuttings particles on the screen surface is prolonged. The improved particle velocity helps to spread the cuttings material along the screen surface, reduce the number of material layers, increase the effective screening area, and improve the screening efficiency. At the same time, it is beneficial to reduce the contact time between cuttings particles and the screen surface, thereby lowering the mis-screening rate. When the vibration amplitude is 3 mm, the average velocity range of cuttings particles is 0.42 m/s to 0.65 m/s. At this time, the vibration amplitude of the screen body is too large, resulting in an increase in the linear reciprocating motion velocity of cuttings particles. The contact time between particles and the screen surface is too short, which is not conducive to improving the screening efficiency. Additionally, the excessively large spreading area of cuttings particles on the screen surface enhances their perforation ability, which is not conducive to reducing the mis-screening rate.

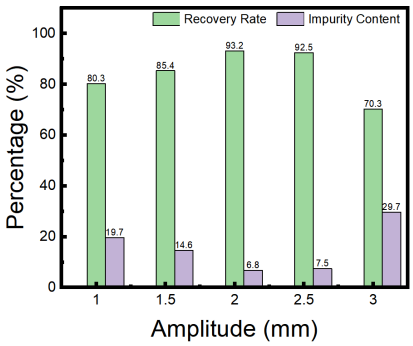

Fig 9. Particle Recovery Rate under Different Vibration Amplitudes

ISSN: 2688-8645

Fig. 9 is a bar chart of the recovery rate and impurity content of the sand washer under different vibration amplitudes. As can be seen from the figure, the cuttings recovery rate first increases and then decreases with the increase of the screen mesh vibration amplitude. When the vibration amplitude is 2 mm, the recovery rate reaches the maximum value of 93.2%. The impurity content of cuttings first decreases and then increases significantly with the increase of the screen mesh vibration amplitude. When the vibration amplitude is 2 mm, the impurity content reaches the minimum value of 6.8%.

Analysis: When the screen mesh amplitude is small, the particles on the screen surface obtain less energy during the screen's operation. The particles cannot be lifted, leading to the accumulation and blockage of large-sized particles on the screen surface. Small-sized cuttings particles are unable to pass through the screen holes, resulting in a naturally low particle recovery rate. When the amplitude is 1 mm, the recovery rate is 80.3%. With the increase of the screen mesh amplitude, the energy acquired by particles during the screen's operation increases gradually. The motion state of particles on the screen surface becomes more intense, and the looseness between particles is greatly enhanced, which is very conducive to the stratification and screening of small particles. Consequently, the number of small-sized cuttings particles passing through the screen mesh increases significantly, and the particle recovery rate rises sharply. As the screen mesh amplitude continues to increase, the motion velocity of particles on the screen surface gradually increases. When the screen mesh amplitude ranges from 1.5 mm to 2 mm, the looseness between particles is very significant, and the average motion velocity of particles on the screen surface is still relatively small (within 0.43 m/s). Therefore, the recovery rate of cuttings particles remains at a very high level, around 93.2%. However, as the amplitude increases from 2.5 mm to 3 mm, the particle motion velocity becomes increasingly high. With the fixed screen mesh length, the contact opportunities between particles and the screen mesh decrease, and the number of cuttings particles passing through the screen holes also decreases accordingly. Thus, the recovery rate of cuttings particles drops from 92.5% to 70.3%.

3.1.3. Influence of Screen Mesh Inclination Angle on Screening Efficiency

When screening cuttings particles, the screen surface is generally installed at an incline to ensure that the particles entering the sand washer are screened out as quickly as possible. Different inclination angles result in different screening efficiencies and processing capacities. Fig. 10 is a schematic diagram of force analysis when the screen surface inclination angle is α. As can be seen from the figure, when particles continuously fall onto the screen mesh, the forces acting on them are mainly divided into two parts: the contact interaction between particles and the screen mesh, and the contact interaction between particles themselves. The cuttings particles falling onto the screen mesh cannot pass through the screen holes, while a small part of the particles get stuck in the screen holes[38].

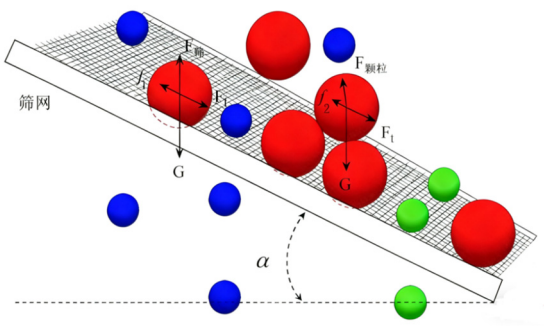

Fig 10. Schematic Diagram of Force Analysis

Among them, the screen holes exert a resistance force Fscreen on the particles, and its component force along the screen surface is f1.As particles continuously fall, accumulation and blockage occur on the screen surface, and particles also exert a resistance force Fparticle on

ISSN: 2688-8645

each other, with its component force along the screen surface being f2.Through analysis, it can be concluded that the component forces f1 and f2 are the primary factors hindering particle falling.The driving force for particle falling is provided by the particles' own gravity.The component force of the particles' gravity interacts with the component forces of the resistance they experience, ultimately determining whether the particles can roll off the screen mesh.

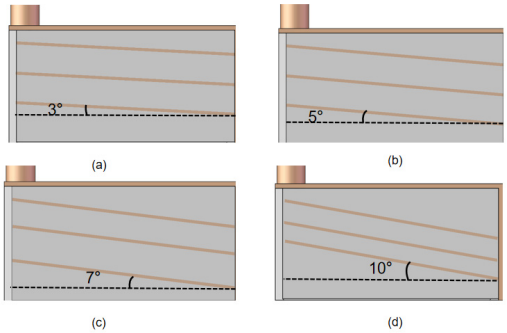

Fig 11. Screen Mesh under Different Inclination Angles

During the simulation, the screen surface inclination angle is one of the important factors affecting the sand washer's screening of cuttings particles. When screening cuttings particles, the screen surface is mostly installed at an incline to facilitate the rapid discharge of particles after screening. Different screen surface inclination angles result in different screening efficiencies of the sand washer. To explore how the screen surface inclination angle affects the particle screening process, four groups of simulation tests were designed with the sand washer's screen mesh vibration amplitude fixed at 2 mm and vibration frequency at 8 Hz. The screen surface inclination angles were set to 3°, 5°, 7°, and 10° respectively, as shown in Fig. 11.

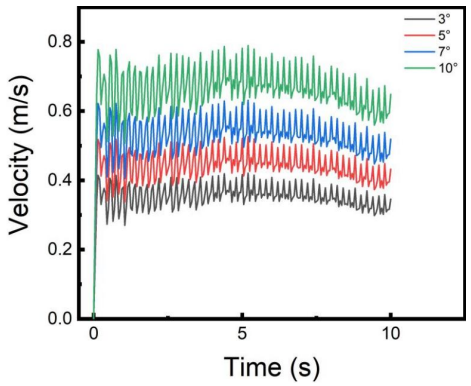

Fig 12. Average Particle Velocity under Different Inclination Angles

As shown in Fig. 12, it is a curve chart of the average velocity of cuttings particles at different screen surface inclination angles. When the screen surface inclination angle is 3°, the average velocity range of cuttings particles is 0.23 m/s to 0.38 m/s. At this time, the screen surface inclination angle is too small, resulting in insufficient gravitational sliding force on the cuttings particles. Materials are prone to accumulate on the screen surface, which is not conducive to improving the screening efficiency. The advancing speed of cuttings particles downward along the screen surface is too slow, and the contact time with the screen surface is excessively long, which will increase the mis-screening rate. When the screen surface inclination angle is 5°, the average velocity range of cuttings particles is 0.38 m/s to 0.49 m/s. With the increase of the screen surface inclination angle, the gravitational sliding force on the cuttings particles increases. Materials are easy to spread downward along the screen surface, expanding the effective screening area and improving the screening efficiency. The advancing speed of

ISSN: 2688-8645

cuttings particles downward along the inclined plane accelerates, reducing the contact time, which is conducive to lowering the mis-screening rate. When the screen surface inclination angle is 7°, the average velocity range of cuttings particles is 0.46 m/s to 0.61 m/s. An excessively large screen surface inclination angle leads to excessive gravitational sliding force on the cuttings particles. The advancing speed of cuttings particles downward along the screen surface is too fast, resulting in too short screening time and insufficient number of screen holes passed by the particles, which is not conducive to improving the screening efficiency. Cuttings particles on the upper layer of the material pile are prone to projectile motion and pass through the screen holes when contacting the screen surface, which will increase the mis-screening rate. When the screen surface inclination angle is 10°, the average velocity range of cuttings particles is 0.58 m/s to 0.77 m/s. The advancing speed of cuttings particles downward along the screen surface is too fast, making it difficult for materials to be evenly distributed on the screen surface. It is easy to have serious accumulation of cuttings particles in some areas of the screen surface while almost no particles in other areas, which further damages the effective screening area and makes the mis-screening more serious.

Fig. 13 is a bar chart of the recovery rate and impurity content of cuttings particles screened by the sand washer under different inclination angles. As can be seen from the figure, the recovery rate of cuttings first increases and then decreases rapidly with the increase of the screen mesh inclination angle. When the screen mesh inclination angle is 5°, the recovery rate reaches the maximum value of 86.5%. The impurity content of cuttings particles first decreases and then increases significantly with the increase of the screen mesh inclination angle. When the screen mesh inclination angle is 5°, the impurity content reaches the minimum value of 13.5%.

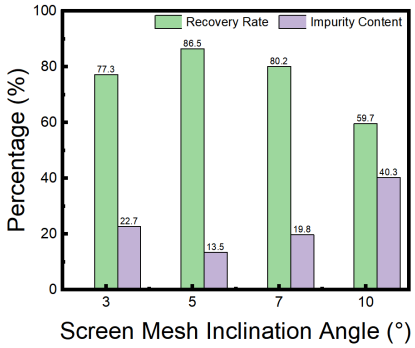

Fig 13. Cuttings Recovery Rate under Different Inclination Angles

Analysis: When the screen mesh inclination angle is 3°, the screen surface tilt is slight. The downward sliding driving force of cuttings particles on the screen surface is weak, and their movement speed is relatively slow, leading to easy stacking and blocking between particles. Large-sized particles tend to accumulate locally on the screen surface, while small-sized particles are trapped among large particles and struggle to contact and pass through the screen holes. Thus, the screening efficiency of small-sized cuttings is low, with a final recovery rate of only 77.3%. Meanwhile, the un-screened small particles are mixed with large particles, resulting in an impurity content of 22.7%.When the inclination angle increases to 5°, the gravitational component force brought by the screen surface tilt is enhanced, and the particle sliding driving force is improved. On one hand, the accumulation state of large particles is broken, the looseness between particles is increased, and small-sized particles are more likely to be exposed from the gaps of large particles and contact the screen holes. On the other hand, the moderate sliding speed allows particles to stay on the screen surface long enough to complete screening. Therefore, the number of small-sized cuttings passing through the screen increases significantly, the recovery rate rises to 86.5%, and the rapid sliding of large particles off the screen surface and the full screening of small particles also reduce the residual

ISSN: 2688-8645

impurities on the screen surface, lowering the impurity content to 13.5%.When the inclination angle further increases to 7°, the particle sliding speed accelerates, but it is still within a controllable range. It will not cause accumulation due to too slow speed nor make particles jump away from the screen holes due to too fast speed. Particles can still maintain a short residence state during movement on the screen surface, and the screening process of small-sized particles proceeds basically smoothly. Thus, the recovery rate remains at a relatively high level of 80.2%, and the impurity content is also kept in a low range of 19.8%.When the inclination angle increases to 10°, the particle sliding speed exceeds the reasonable threshold. The excessive gravitational component force causes the particles to slide quickly on the screen surface, and the contact time with the screen mesh is greatly shortened. Small-sized particles slide off the screen surface together with large particles before contacting the screen holes, and the screening process is severely compressed. At the same time, the excessively fast speed intensifies collisions between particles, making small particles more likely to be trapped and carried away by large particles. Therefore, the number of small-sized cuttings passing through the screen drops sharply, the recovery rate significantly decreases to 59.7%, and a large number of un-screened small particles are mixed in the product, leading to the impurity content rising to 40.3%.

3.2. Parameter Optimization Based on Response Surface Methodology

3.2.1. Design Variables and Optimization Objectives

Based on the above analysis, it can be concluded that the efficiency of the sand washer in screening cuttings changes with variations in screen mesh vibration frequency, amplitude, and inclination angle. To achieve better screening efficiency, it is necessary to obtain the optimal parameters for screen mesh vibration. The screening efficiency under different factors obtained through numerical simulation is taken as the objective function for optimization. As indicated earlier, the optimization range of vibration frequency is 6~15 Hz, the optimization range of amplitude is 1~3 mm, and the optimization range of vibration inclination angle is 3°~10°. The level data of the factors are shown in Table 3.

Table 3. Factor Level Data Sheet

Group count	Frequency(Hz)	Amplitude(mm)	Inclination(°)
1	6	1	3
2	8	1.5	5
3	10	2	7
4	12	2.5	10
5	15	3	

In this paper, vibration frequency, amplitude, and vibration inclination angle are selected as the design variables for this multi-objective optimization, aiming to obtain the optimal combination of these three factors while keeping the overall dimensions of the sand washer unchanged. A test plan design table is generated using test design software, and numerical simulations are conducted with parameter settings in Fluent software [39-40]. The calculated cuttings screening efficiency is filled into the table. The test plan design and results are shown in Table 4.

3.2.2. Response Model Establishment and Significance Analysis

A second-order polynomial function regression fitting was performed on the screening efficiency results and parameters in Table 4. The obtained second-order polynomial regression equation is as follows:

ISSN: 2688-8645

$$Y= --116.93291+8.70103X_1+98.24952X_2+23.23258X_3-2.57519X_1X_2 -0.68337\ X_1X_3 + 0.63595X_2X_3+0.024765X_1^2-18.67881X_2^2-1.53703X_3$$

Table 4. Optimization Scheme Parameter Table

experimental sequence	Frequency (Hz)	Amplitude (mm)	Inclination (°)	Efficiency (%)
1	6	1	3	42.1
2	6	2	5	79.3
3	10	3	7	76.5
4	8	1.5	5	81.5
5	8	2	7	92.3
6	6	1.5	10	70.1
7	12	3	5	67.5
8	12	2	5	85.9
9	10	1.5	7	74.3
10	8	2.5	5	87.7
11	10	1	7	70.6
12	15	3	7	62.8
13	8	3	10	55.3
14	8	2	10	77.6
15	15	2	7	81.2
16	12	1.5	7	84.5
17	10	1.5	10	60.4

In the formula,X_1,X_2,X_3 and Y represent the corresponding data of vibration frequency, amplitude, screen mesh inclination angle, and screening efficiency, respectively. The P-value in the function parameters obtained by regression fitting indicates the significance of the correlation coefficient. A P-value less than 0.01 means the parameter is highly significant for the target; a P-value less than 0.05 indicates the parameter is significant for the target; while a P-value greater than 0.05 means the parameter is not significant for the target. The analysis of variance for this model is shown in Table 5.

Table 5. Analysis of Variance Table

Type	Quadratic Sum	Free Degree,	Mean Square Deviation	F Value	P Value
Model	3009.33	9	334.37	11.20	0.0022
X_1	6.88	1	6.88	0.23	0.0646
X_2	1.80	1	1.80	0.060	0.0813
X_3	177.49	1	177.49	5.95	0.0448
X_1X_2	90.38	1	90.38	3.03	0.1254
X_1X_3	199.26	1	199.26	6.68	0.0363
X_2X_3	7.52	1	7.52	0.25	0.6312
X_1^2	0.16	1	0.16	5.376E-003	0.9436
X_2^2	432.34	1	432.34	14.49	0.0067
X_3^2	325.08	1	325.08	10.89	0.0131
residual	208.90	7	29.84	—	—
mismatch	185.75	6	30.96	1.34	0.5793
total difference	23.12	1	23.12	—	—
R^2	—	—	0.8912	—	—

For individual terms in the model, whether the term has a significant relationship with the target is also judged by comparing the P-value with 0.05. As can be seen from Table 5, the

ISSN: 2688-8645

significant terms in the degassing efficiency model are X_2,X_3,X_1X_3, X_2^2,and X_3^2. The coefficient of determination R^2 of the model is 0.8912, indicating a good fit between the response model and the simulation results. A response surface was established based on this model for analysis.

3.2.3. Analysis of Response Surface Optimization Results

Response surface relationship diagrams were plotted based on the response surface model established in the previous section. The response relationship between vibration frequency and amplitude on screening efficiency is shown in Fig. 14.

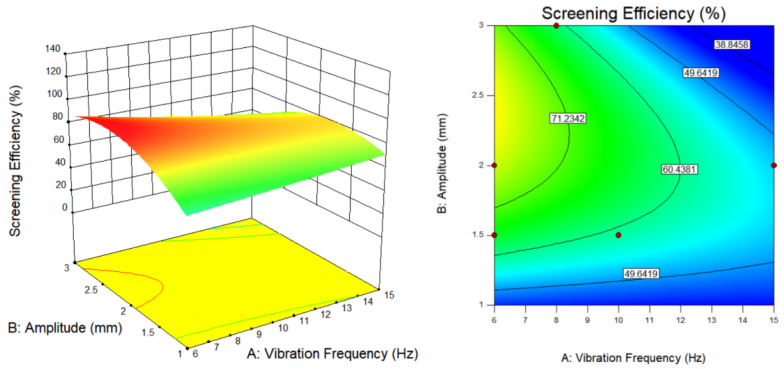

Fig 14. The response relationship between vibration frequency and amplitude on screening efficiency

As can be seen from Fig. 14, with the increase of vibration frequency, the screening efficiency shows an obvious overall upward trend. When the frequency is in the range of 6~10 Hz, the efficiency increases rapidly; after the frequency exceeds 10 Hz, the upward trend of efficiency gradually flattens and finally tends to a stable high level. This is because a higher vibration frequency can enhance the looseness of particles on the screen surface, reduce the probability of large particles blocking the screen holes, and thus improve the screening efficiency of small-sized particles. The influence of amplitude on screening efficiency is relatively gentle: when the amplitude is in the range of 1.5~2.5 mm, combined with a higher vibration frequency, the screening efficiency can be maintained at a high level; when the amplitude is too small (less than 1.5 mm) or exceeds 2.5 mm, even if the frequency is high, the efficiency improvement will be limited. At this time, too small amplitude leads to insufficient particle loosening, and too large amplitude makes particles easy to be thrown off the screen surface, reducing the screening time.

Response surface relationship diagrams were plotted based on the response surface model established in the previous section. The response relationship between screen mesh inclination angle and amplitude on screening efficiency is shown in Fig. 15.

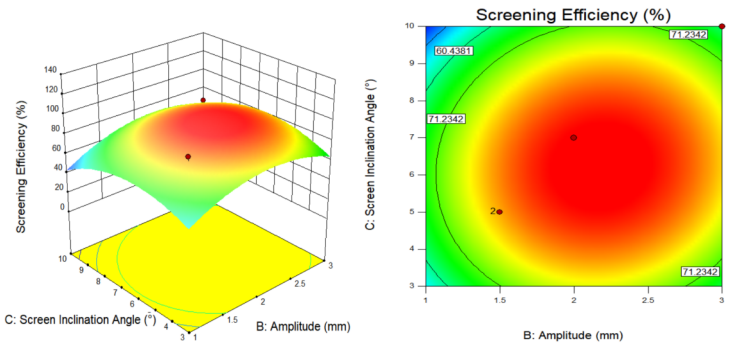

Fig 15. The response relationship between screen mesh inclination angle and amplitude on screening efficiency

ISSN: 2688-8645

Under the condition that the vibration frequency is fixed at 8 Hz, the screen mesh inclination angle and amplitude show a synergistic "first increasing and then decreasing" change law on the screening efficiency: when the screen mesh inclination angle is in the range of 5° to 9° and the amplitude is in the range of 1.5 mm to 2.5 mm, the screening efficiency is maintained at a high level. Among them, the parameter combination of a screen mesh inclination angle of about 7° and an amplitude of about 2 mm corresponds to the efficiency peak area; if the screen mesh inclination angle deviates from the range of 5° to 9°, or the amplitude deviates from the range of 1.5 mm to 2.5 mm, the screening efficiency will decrease significantly. The core mechanism of this law lies in: too small a screen mesh inclination angle will lead to particle accumulation and blockage on the screen surface, while too large an angle will accelerate the particle sliding speed and shorten the screening contact time; insufficient amplitude will reduce the particle looseness, and excessive amplitude will reduce the effective contact time between particles and the screen surface. Only when the screen mesh inclination angle and amplitude are in the adaptive range can the loose state of particles and sufficient screening time be guaranteed simultaneously, thereby achieving high screening efficiency.

Response surface relationship diagrams were plotted based on the response surface model established in the previous section. The response relationship between screen mesh inclination angle and vibration frequency on screening efficiency is shown in Fig. 16.

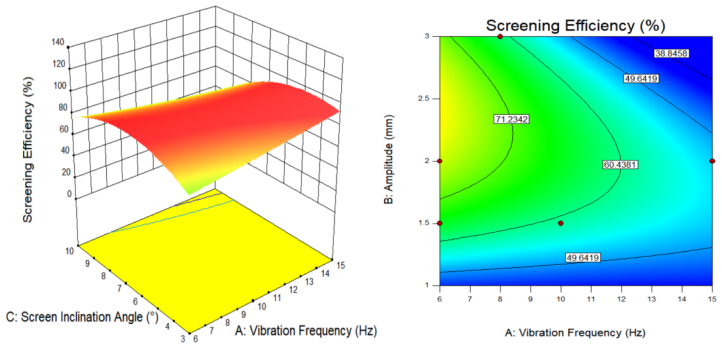

Fig 16. The response relationship between screen mesh inclination angle and vibration frequency on screening efficiency

Under the condition that the amplitude is fixed at 2 mm, the screen mesh inclination angle and vibration frequency exhibit a significant synergistic effect on the screening efficiency: as the vibration frequency increases, the screening efficiency shows an overall upward trend, while the adaptive range of the screen mesh inclination angle presents dynamic characteristics with frequency changes. In the higher vibration frequency range, the screening efficiency remains at a high level when the screen mesh inclination angle is between 7°and 9°; if the vibration frequency is relatively low, it is difficult to improve the screening efficiency even by adjusting the screen mesh inclination angle. The mechanism is as follows: the increase in vibration frequency can enhance the looseness of particles on the screen surface and reduce the probability of large particles blocking the screen holes. An adaptive screen mesh inclination angle can balance the sliding speed and screening time of particles, avoiding particle accumulation caused by an excessively small inclination angle or rapid particle sliding due to an excessively large inclination angle. Under their synergistic effect, when the vibration frequency is in a higher range and the screen mesh inclination angle is within a reasonable range, particles can not only be fully loosened to expose small-sized components but also maintain sufficient contact time with the screen surface to complete screening, thereby achieving high screening efficiency.

With the goal of ensuring the maximum screening efficiency, the constructed response surface model was solved using an optimization function. Based on the interactive response

ISSN: 2688-8645

relationships among the three types of parameters (vibration frequency, amplitude, and screen mesh inclination angle), it can be concluded that under different fixed parameter conditions, the synergistic effect of each variable on the screening efficiency presents a clear law: when the screen mesh inclination angle is fixed at 7°, the combination of a vibration frequency of 10~15 Hz and an amplitude of 1.5~2.5 mm can significantly improve the screening efficiency; when the vibration frequency is fixed at 8 Hz, the adaptive range of a screen mesh inclination angle of 5°~9° and an amplitude of 1.5~2.5 mm corresponds to the efficiency peak; when the amplitude is fixed at 2 mm, the synergistic effect of a higher vibration frequency and a screen mesh inclination angle of 7°~9° can ensure the loose screening of particles. Finally, the optimal parameter combination for the maximum screening efficiency of the vibrating screen is obtained as follows: vibration frequency of 10~15 Hz, amplitude of 1.5~2.5 mm, and screen mesh inclination angle of 5°~9°. The model predicts that under the action of this optimal parameter combination, the vibrating screen can simultaneously balance the looseness of particles and the screening time, effectively avoiding the problems of accumulation, blockage, or excessive sliding, and the screening efficiency can be maintained at a high level.

4. Experimental Verification

To verify the correctness of the simulation, an experiment on vibrating screening of cuttings particles by the sand washer is required. The overall 3D model of the sand washer is shown in the figure. The experimental device for vibrating screening of the sand washer in this paper mainly consists of a mud deflector, a cuttings feed port, a clean water spray head, a water pump, a particle inlet, a water tank, and several pipelines. The physical diagram of the sand washer used in the experiment and the cuttings particle samples are shown in Fig. 17.

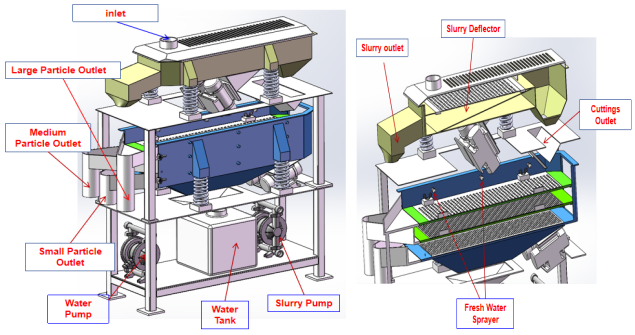

Fig 17. 3D Modeling Diagram of the Sand Washer

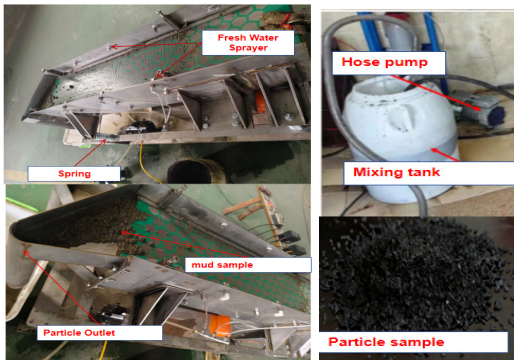

Fig 18. Physical Diagram of the Sand Washer Experimental Device and Cuttings Particle Samples

4.1. Influence of Different Flow Rates on Screening Performance

During the experiment, the inlet velocity of the drilling fluid in the sand washer was set to 4 m/s, the particle size was 2 mm, and the drilling fluid densities were 1.8 g/cm^3 and 2.2 g/cm^3

ISSN: 2688-8645

respectively. Fig. 19 shows the comparison curves of the screening efficiency of the sand washer when the drilling fluid densities are 1.8 g/cm^3 and 2.2 g/cm^3. It can be seen that as the particle content increases, the screening efficiency of the sand washer gradually increases, which is consistent with the results of the simulation analysis. At the same time, the simulation results of the two control groups indicate that the experimental data are often slightly lower than the theoretical data, which is also roughly consistent with practical experience.

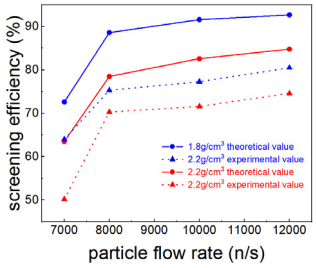

Fig 19. Comparison of Experimental and Simulation Results Under Different Particle Flow Rates

5. Conclusion

Aiming at the problem of insufficient cuttings screening efficiency of sand washers in petroleum drilling and mud logging engineering, this paper takes the sand washer vibration model as the research carrier, adopts the CFD-DEM method to simulate the screening process of cuttings-containing drilling fluid in the sand washer, and studies the influence of different structural parameters on the vibration screening performance of the sand washer. Secondly, the response surface methodology is used to optimize the vibration parameters. Finally, the reliability of the research conclusions is verified through experiments.

The main research results and conclusions are as follows:

(1) Based on the actual structure of the sand washer vibrating screen, a scaled-down simplified physical model is established. The Launder-Spalding standard k-ε model is used to describe the turbulent flow characteristics of the drilling fluid, and the Hertz non-slip contact model is combined to simulate the collision and motion behavior of cuttings particles. The dynamic interaction between the fluid field and the particle field is realized through a one-way coupling strategy. Grid independence verification shows that when the number of grids is 624,362, the calculation result of the average particle velocity converges, balancing calculation accuracy and efficiency, and providing a reliable numerical simulation platform for subsequent parameter analysis.

(2) The screening efficiency presents a non-linear change of first increasing and then decreasing with frequency, and 8 Hz is the critical threshold. When the frequency is in the range of 6~8 Hz, the intensity of particle motion increases, the contact frequency with the screen increases by 37%, the screening rate of small-sized particles increases significantly, and the efficiency rises from 64.2% to the peak of 92.8%. When the frequency is 8~15 Hz, the average particle velocity increases, and the excessive kinetic energy causes particles to slide off the screen before fully screening, resulting in the efficiency dropping to 78.6%. The optimal screening effect is achieved when the amplitude is 2 mm. When the amplitude is 1~2 mm, the vibration energy obtained by particles increases from 0.28 J to 0.45 J, the looseness is improved, the blockage of screen holes by large particles is alleviated, and the efficiency increases by 16.9%. When the amplitude is 2~3 mm, the proportion of time that particles are thrown off the screen surface increases from 12% to 25%, the effective contact time is shortened, and the efficiency drops to 70.3%. The balance critical point between particle sliding power and screening time is about 5°. When the inclination angle is slightly lower, the component of

particle gravity along the screen surface increases from 0.87 N to 1.12 N, the accumulation phenomenon is alleviated, and the efficiency rises from 77.3% to 86.5%. When the inclination angle is slightly higher, the average sliding velocity of particles increases from 0.38 m/s to 0.77 m/s, the screening path is shortened, and the efficiency drops sharply to 59.7%.

(3) The optimal parameter range based on the response surface methodology is obtained. Taking frequency, amplitude, and inclination angle as variables, a quadratic regression model is fitted through 17 sets of simulation data. Significance test shows that the quadratic term of amplitude, the quadratic term of inclination angle, and the interaction term of frequency and inclination angle have significant effects. The optimized optimal range is: frequency 10~15 Hz, amplitude 1.5~2.5 mm, and inclination angle 5°~9°, within which the screening efficiency is stably greater than 90%.

(4) A scaled experimental platform is built. Comparative experiments show that the variation trend of experimental values is consistent with that of simulation values. The experimental efficiency reaches 94.2% under the optimal parameter range, which is very close to the predicted value, confirming the engineering practicality of the model and the optimization scheme.

References

[1] Cochran G V, Gand R, Blossom B, Standard measurement of cardiac function indexes. Journal of Medical Ultrasonics. 33(1) (2006) 123-127.

[2] Cheng L, Ye X, Wang H, et al., A New Gas Logging Method Based on Semipermeable Film Degasser and Infrared Spectrum. Petrophysics 65(4) (2024) 17.

[3] Bravo M C, Cely A, Yerkinkyzy G, et al., A Novel Method to Map Heavy Oil Viscosity From Standard Mud Gas – A Field Case From the Peregrino Field. Petrophysics, 65(4) (2024) 12.

[4] Wu Z, APPLICATION OF FUZZY PATTERN RECOGNITION METHOD TO GAS LOGGING DATA INTERPRETATION. NATURAL GAS INDUSTRY, 20(4) (2000) 30-32.

[5] Li S, Cai W, Chen J,et al., Numerical study on the flow and heat transfer characteristics of forced convective condensation with propane in a spiral pipe. International Journal of Heat and Mass Transfer 117 (2018) 1169-1187.

[6] S.A. Marzouk, Fahad Awjah Almehmadi, et al., Effects of extended pin fins on the hydrothermal performance of double pipe heat exchanger. Thermal Science and Engineering Progress 55 (2024) 102915.

[7] Shang Mao, Tao Zhou, Dong Wei, Modeling of heat transfer of supercritical water in helical finned double pipe,International Journal of Heat and Mass Transfer 180 (2021) 121754.

[8] Wang D, Zang R, Wang G, et al., Numerical study of heat transfer performance and flow characteristic of water in a multi-wound pipe heat exchanger. Thermal Science and Engineering Progress 52 (2024) 102683.

[9] Zhang D, Zhao L, Dong H, et al., Experimental study on heat transfer and flow resistance characteristics of integral rolled spiral finned tube bundles heat exchangers. Case Studies in Thermal Engineering 52 (2023) 103689.

[10] Naim BA, Dheyaa JJ, Saman A, et al., Numerical exploration of the impact of fluid type in a uniquely designed shell and spiral tube heat exchanger. Case Studies in Thermal Engineering 61 (2024) 104798.

[11] Hossein K, Younes S, Pourya O, Comparison of heat transfer characteristics of a heat exchanger with straight helical tube and a heat exchanger with coiled flow reverser[J]. Applied Thermal Engineering 253 (2024) 123772.

[12] Wei-mei Quan, Wen-jing Sun, et al., Flow dynamics and heat transfer enhancement of single pulsed jet impingement in a confined crossflow channel, International Journal of Heat and Mass Transfer. 250 (2025) 127286.

[13] Soumaya Sokakini, Jules Voguelin Simo Tala, et al., Heat transfer enhancement in shell and tube Latent Heat Thermal Energy Storage units for waste heat recovery applications: A 3D numerical study on melting–solidification kinetics. Applied Thermal Engineering 274 (2025) 126564.

[14] Xiaoqin Liu, Min Wang, Hengheng Liu, et al., Numerical analysis on heat transfer enhancement of wavy fin-tube heat exchangers for air-conditioning applications. Applied Thermal Engineering.199 (2021) 117597.

[15] Antonio C. Caputo, Alessandro Federici et al., On the selection of design methodology for shell-and-tube heat exchangers optimization problems. Thermal Science and Engineering Progress34 (2022) 101384.

[16] Samet Gürgen, Shell and tube heat exchanger optimization: A critical literature assessment and fairness-based comparative performance analysis of meta-heuristic algorithms. Case Studies in Thermal Engineering, 72 (2025)106405.

[17] He Dong, Zhile Yang, Hangcheng Yu, et al., A novel balanced teaching-learning-based optimization algorithm for optimal design of high efficiency plate-fin heat exchanger. Applied Thermal Engineering, 256 (2024) 124052.

[18] Huang X, Chen S, Zhou T, Sun Y, A Review of Genetic Algorithms for Solving Flexible Job Shop Scheduling Problems. Computer Integrated Manufacturing Systems 28 (2) (2022) 536-551.

[19] Qin Y, Tang T, Zhang L, Research on Dynamic Load Identification Based on Improved Genetic Algorithm, Vibration testing and diagnosis 45 (1) (2025) 146-153.

[20] Cheng XX, Numerical simulation of finned tube heat exchanger and multi-objective optimization design of structural parameters, East China University of Science and Technology, Nanchang, China (2021).

[21] Zhang T, Chen L, Wang J, Multi-objective optimization of elliptical tube fin heat exchangers based on neural networks and genetic algorithm. Energy 269 (2023) 126729.

[22] Petrovic M, Fukui K, Kominami K, Numerical and experimental performance investigation of a heat exchanger designed using topologically optimized fins. Applied Thermal Engineering 218 (2023) 119232.

[23] Li Y, Xu H, Guo P. CFD-DEM study on mixing and segregation characteristics of binary particles in a fluidized bed with secondary air, Adv. Powder Technol. 36(7) (2025) 104909.

[24] Qian Y, Usher S P, Scales P J, et al. Numerical simulation of particle consolidation under compression and shear based on the Discrete Element method. Adv. Powder Technol. 35(12) (2024) 104722.

[25] Liang Y, Cheng T, Li Q, Liu Q, Li J, Ma S, Jiang X, Wang H, Fu P, CFD-DEM simulation of cyclone self-rotation drying: Particle high-speed self-rotation and heat transfer. Energy 290 (2024) 130277.

[26] Shan Y, Jing J, Zhang Z, Sun J, Wang N, Zhuang L, Guo Y, Investigation of erosion behavior of particle-fluid flow in offshore platform T-pipes. International Journal of Pressure Vessels and Piping 209 (2024) 105174.

[27] Mazen M O, Faris S B, Thiana A S, Siamack A SExperimental and numerical assessments on solid particle erosion in upward vertical-horizontal and horizontal-vertical downward elbows for multiphase and gas-sand flows. Wear 524 (2023) 204812.

[28] Ma H, Zhou L, Liu Z, Chen M, Xia X, Zhao Y, A review of recent development for the CFD-DEM investigations of non-spherical particles. Powder Technology 412 (2022) 117972.

[29] Li Z, Chen H, Wu Y, Xu Z, Shi H, Zhang P, CFD-DEM analysis of hydraulic conveying of non-spherical particles through a vertical-bend-horizontal pipeline. Powder Technology 434 (2024) 119361.

[30] Meng HC, Ludema KC, Wear models and predictive equations:their form and content. Wear 181 (1995) 443-457.

[31] Vlasák P, Chára Z, Krupička J, Jiří K, Experimental investigation of coarse particles-water mixture flow in horizontal and inclined pipes. Journal of Hydrology and Hydromechanics 62 (3) (2014) 241-247.

[32] Alajbegovic A, Phase distribution and turbulence structure for solid/fluid upflow in a pipe. International Journal of Multiphase Flow 20 (3) (1994) 453-479.

ISSN: 2688-8645

[33] Sun Y, Chen Y, Wang B, Wu Y, Simulation Analysis of Corrosion of 90° Elbow in Heavy Oil Transportation Pipelines. Journal of Beijing University of Chemical Technology 47 (6) (2020) 40-46.

[34] Zhu HJ, Wang J, Ba B, Wu Z, Wang W, Numerical investigation of flow erosion and flow induced displacement of gas well relief line. Journal of Loss Prevention in the Process Industries 37 (2015) 19–32.

[35] Lin N, Lan HQ, Xu YG, Dong SH, Barber G Effect of the gas –solid two-phase flow velocity on elbow erosion. Journal of Natural Gas Science and Engineering 26 (2015) 581–586.

[36] Zhang Y, Reuterfors E P, Mclaury BS, Comparison of computed and measured particle velocities and erosion in water and air flows. Wear 263 (1) (2007) 330–338.

[37] Werbos PJ BEYOND REGRESSION: NEW TOOLS FOR PREDICTION AND ANALYSIS IN THE BEHAVIORAL SCIENCES, Harvard University, Cambridge, MA (1975).

[38] Vasconcelos S, Emerson HD, Mariani VC, Coelho LS Design of heat exchangers using Falcon Optimization Algorithm. Applied Thermal Engineering 156 (2019) 119-144.

[39] Q.Y. Chen, T. Xiong, X.Z. Zhang, P. Jiang, Study of the hydraulic transport of non-spherical particles in a pipeline based on the CFD-DEM, Engineering Applications of Computational Fluid Mechanics 14 (1) (2020) 53-69.

[40] M.M. Zhou, S. Wang, S.B. Kuang, K. Luo, J.R. Fan, A.B. Yu, CFD-DEM modelling of hydraulic conveying of solid particles in a vertical pipe, Powder Technology 354 (2019) 893-905.